RAA 2020 Vol. **20** No. **6**, 87(10pp) doi: 10.1088/1674–4527/20/6/87

http://www.raa-journal.org *http://iopscience.iop.org/raa*

***R**esearch in*
***A**stronomy and*
***A**strophysics*

Site testing at Muztagh-ata site II: seeing statistics

Jing Xu[1,2], Ali Esamdin[1,2], Jin-Xin Hao[3], Jin-Min Bai[4], Ji Yang[5], Xu Zhou[3], Yong-Qiang Yao[3], Jin-Liang Hou[6], Guang-Xin Pu[1], Guo-Jie Feng[1,2], Chun-Hai Bai[1], Peng Wei[1], Shu-Guo Ma[1], Abudusaimaitijiang Yisikandee[1], Le-Tian Wang[1], Xuan Zhang[1], Liang Ming[1], Lu Ma[1], Jin-Zhong Liu[1], Zi-Huang Cao[2,3], Yong-Heng Zhao[3], Lu Feng[3], Jian-Rong Shi[3], Hua-Lin Chen[7], Chong Pei[7], Xiao-Jun Jiang[3], Jian-Feng Wang[3], Jian-Feng Tian[3], Yan-Jie Xue[3], Jing-Yao Hu[3] and Yun-Ying Jiang[3]

[1] Xinjiang Astronomical Observatory, Chinese Academy of Sciences, Urumqi 830011, China; *xujing@xao.ac.cn; aliyi@xao.ac.cn*
[2] University of Chinese Academy of Sciences, Beijing 100049, China
[3] National Astronomical Observatories, Chinese Academy of Sciences, Beijing 100101, China
[4] Yunnan Observatories, Chinese Academy of Sciences, Kunming 650000, China
[5] Purple Mountain Observatory, Chinese Academy of Sciences, Nanjing 210008, China
[6] Shanghai Astronomical Observatory, Chinese Academy of Sciences, Shanghai 200030, China
[7] Nanjing Institute of Astronomical Optics & Technology, Chinese Academy of Sciences, Nanjing 210008, China

Received 2019 September 2; accepted 2019 November 28

Abstract In this article, we present a detailed analysis of the statistical properties of seeing for the Muztagh-ata site which is a candidate site for hosting the future Chinese Large Optical/infrared Telescope (LOT) project. The measurements were obtained with differential image motion monitors (DIMMs) from April 2017 to November 2018 at different heights during different periods. The median seeings at 11 m and 6 m are very close but significantly different from that on the ground. We mainly analyzed the seeing at 11 m monthly and hourly, having found that the best season for observing was from late autumn to early winter and seeing tended to improve during the night only in autumn. The analysis of the dependence on temperature inversion, wind speed and direction also was made and the best meteorological conditions for seeing are given.

Key words: site-testing — seeing

1 INTRODUCTION

The Muztagh-ata site is one of three potential astronomical locations in western China for hosting the future Large Optical/infrared Telescope (LOT) project. LOT, which is an ambitious project with the goal of constructing a 12 m telescope aiming at frontier scientific research on the nature of dark energy, detecting Earth-like extrasolar planets, supermassive black holes, first stars, etc., was selected in 2015 (Feng et al. 2020). The site assessment campaign was initiated in January 2017 and lasted for more than two years. Climatological properties and optical observing conditions such as sky brightness and amount of clouds at the Muztagh-ata site were reported earlier by Xu et al. (2020a,b) and Cao et al. (2020a,b). In this article, we focus on the seeing conditions at our site.

Image quality is directly related to the statistics of the perturbations of the incoming wavefront. With wavefront sensing methods, wavefront fluctuations can be directly analyzed, providing quantitative information on seeing, independent of the telescope being utilized (Sarazin & Roddier 1990). A differential image motion monitor (DIMM) has become the standard equipment for assessing the atmospheric "seeing" at astronomical sites (Skidmore et al. 2009). The seeing derived from a DIMM is the combined or integrated effect of all contributing optical turbulence along the optical path (Tokovinin 2002). Michel et al. (2003) conducted a study with a DIMM at San Pedro Mártir observatory and yielded a median seeing of 0.60 arcsec during 123 nights in a three-year period. Tian et al. (2016) measured seeing with a DIMM at Delingha station and achieved an overall median seeing of 1.58 arcsec

Table 1 Parameters and Technical Specifications of Two DIMMs

	French DIMM	NIAOT DIMM
Telescope Aperture (mm)	300	304.8
Focal ratio	8	8
Focal length (mm)	2400	1600
Sub-aperture	2	4
Sub-aperture diameter (mm)	51	50
Sub-aperture distance (mm)	240	149
Camera	DMK 33GX 174	Basler aca2040
Exposure method	Adjusted automatically between 0.5 ms and 1000 ms	5 ms or 10 ms
Wavelength (mm)	550	500
Output frequency	1 Seeing value for every 1000 images	1 Seeing value for every minute
Scaling and conversion	Convert to zenith No exposure time scaling No wavelength scaling	Convert to zenith No exposure time scaling

from 2010 to 2012. Furthermore, a DIMM combined with a Multi-Aperture Scintillation Sensor (MASS) was widely employed for optical turbulence profile measurement (Els et al. 2009; Skidmore et al. 2009; Sánchez et al. 2012).

The seeing measurements were conducted at Muztagh-ata site during the period from April 2017 to November 2018. We analyze the seeing data collected by DIMMs and give the global, monthly and hourly statistics. We also present the seeing behavior on different conditions of temperature inversion, wind speed and direction. The layout of this paper is as follows: In Section 2, the working methods of DIMM and our instruments for seeing measurements are briefly described. In Section 3, we introduce how the DIMMs operated at the Muztagh-ata site. In Section 4, we firstly show a comparison result between the two DIMMs, then we provide the statistics on seeing at different heights during different periods and at last we focus on the 11 m seeing and detail its statistics from aspects of monthly and hourly trends. Section 5 features the relation between seeing and some meteorological parameters such as temperature inversion, wind speed and direction. Conclusions are given in Section 6.

2 SEEING AND SEEING MEASUREMENT

Atmospheric turbulence is usually studied through seeing (ε). The relation between ε, Fried parameter γ_0 and the turbulence integral is expressed as (Roddier 1981)

$$\varepsilon = 0.98\frac{\lambda}{\gamma_0} = 5.25\lambda^{-1/5}[\int_0^\infty C_N^2\, dh]^{3/5}\,, \qquad (1)$$

where λ is the wavelength and $\int_0^\infty C_N^2(h)\, dh$ is the optical turbulence energy profile, C_N^2 is refractive index structure constant and h represents altitude.

The central wavelength of light measured by the DIMM is $\lambda = 0.5$ μm and the final results have been converted for the direction of observation to zenith angle according to the following relation

$$\varepsilon_0 = \varepsilon_{0\zeta} \cdot (\cos\zeta)^{\frac{3}{5}}\,, \qquad (2)$$

where ζ is the zenith angle, ε_0 is the seeing at zenith and $\varepsilon_{0\zeta}$ is the seeing as determined by DIMM. The DIMM measurements of the positions of the image centers of stars are made from short exposure images. The exposure time is automatically selected by software according to star magnitude. We focus on the integrated seeing down to the level of the DIMM corrected to one air mass and zero exposure time (Els et al. 2009; Skidmore et al. 2009). The Muztagh-ata site was equipped with two DIMMs, one is called a French DIMM and the other one is named a NIAOT DIMM in the following sections. Parameters describing these two DIMMs are summarized in Table 1 (Wang et al. 2020).

Table 2 Operation Time Periods of the Two DIMMs

Starting-Date	French DIMM	NIAOT DIMM
2017.03.12	-	ground
2017.04.15	ground	ground
2017.06.23	11 m	ground
2017.11.15	11 m	6 m
2018.09.21	11 m	11 m

3 SEEING MONITORING AT MUZTAGH-ATA

The seeing measurement task at Muztagh-ata site began in April 2017 and lasted until November 2018. We obtained a median value of 0.83 arcsec from the French DIMM and 0.89 arcsec from the NIAOT DIMM during the whole measurement period. Here we first introduce the two DIMMs' operation during the whole measurement period.

We have built two towers for seeing measurements, with heights of 11 m and 6 m respectively, and no dome for protection as depicted in Figure 1. The difference in heights between the two towers is utilized to explore the effect of difference in heights on seeing values. At first, the observation was conducted on the ground before the

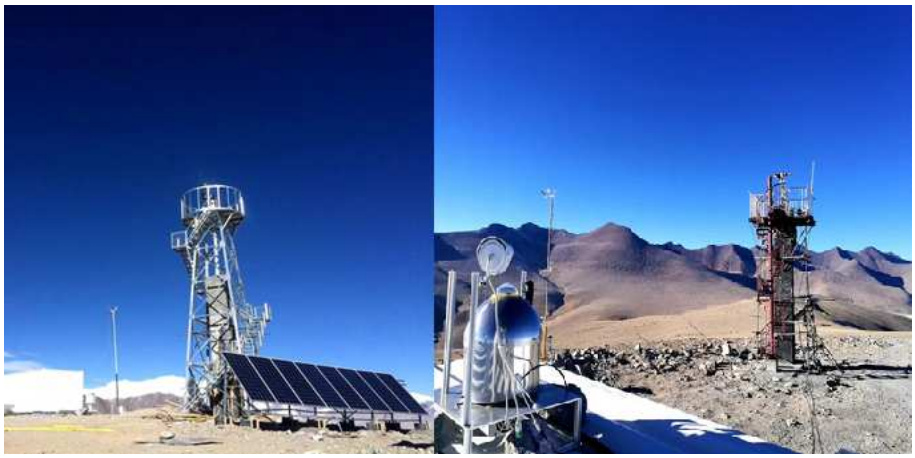

Fig. 1 11-meter tower (*left*) and 6-meter tower (*right*) at Muztagh-ata.

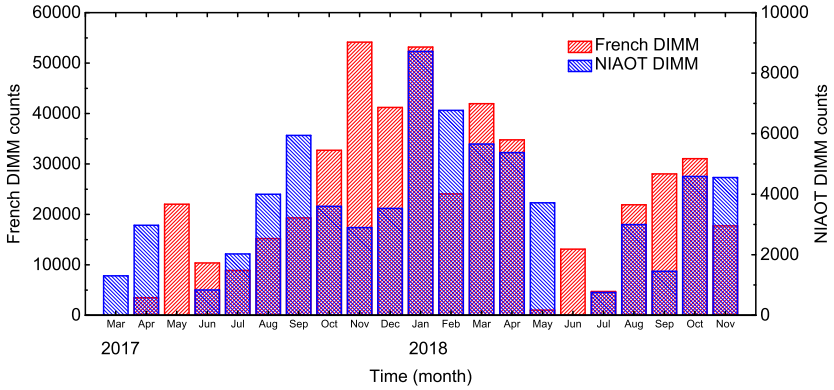

Fig. 2 Total monthly data from March 2017 to June 2018. Patterns: French DIMM (*red*), NIAOT DIMM (*blue*).

two towers were built. Then we moved the two DIMMs to the tops of towers successively. The periods of the two DIMMs running at different heights are as follows: the French DIMM was installed on 2017 April 15. It operated on the ground until 2017 June 23, then we moved it to the top of the 11-meter tower; the NIAOT DIMM was installed on 2017 March 12 and ran on the ground until 2017 November 15, then we moved it to the top of the 6-meter tower. After rebuilding the 11-meter tower, for the purpose of ensuring two DIMMs can be housed on the top of it simultaneously, we installed the NIAOT DIMM on it on 2018 September 21. The two DIMMs were operating at 11 m until 2018 November 20 for comparison. The detailed operation periods and heights of the two DIMMs can be seen in Table 2.

In Figure 2, we present the total data from the two DIMMs for each month during the acquisition period. Because the sample rate of the French DIMM is about five times that of the NIAOT DIMM, we use different axes to represent the data amounts of the two DIMMs, left for French DIMM and right for NIAOT DIMM. It is noteworthy that in May 2018 we rebuilt the 11-meter tower so the amount of data from the French DIMM in that month is relatively smaller. Due to the failure of a CCD and a controller, the NIAOT DIMM did not operate during May 2017 and June 2018.

4 SEEING STATISTICS

4.1 Comparison of Two DIMMs

Because the 11-meter tower could only accommodate one DIMM before being rebuilt, we did a comparison after expanding its platform. The comparison work for the French DIMM and NIAOT DIMM was from 2018 September 21 to 2018 November 20, during which the two DIMMs both were operated at the top of the 11-meter tower. In Figure 3, we show seeing measurements from two nights, from which we can ascertain that the seeing from the French DIMM coincides well with that from the NIAOT DIMM. Since the sampling rate of the French DIMM is about five times that of the NIAOT DIMM, in this comparison work, we firstly find out the nearest moment that the seeing of the French DIMM is closest to that of NIAOT DIMM, then use the median value of a neighborhood of

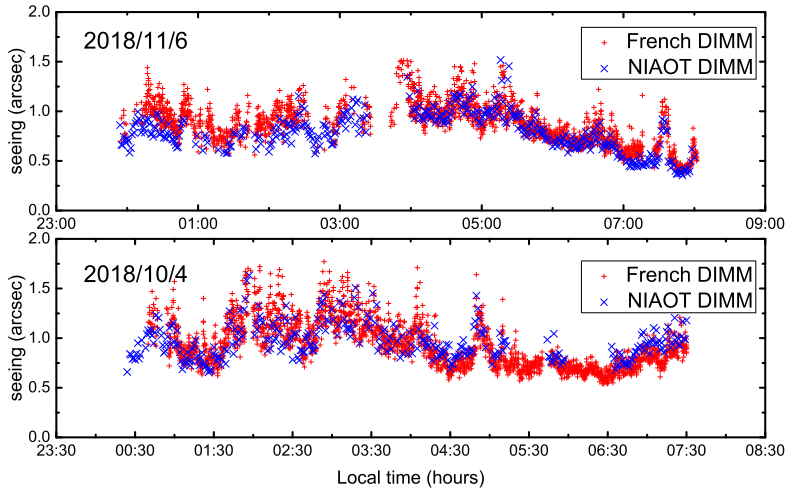

Fig. 3 Example of seeing values from French DIMM (*red crosses*) and NIAOT DIMM (*blue crosses*) at 11 m during two nights.

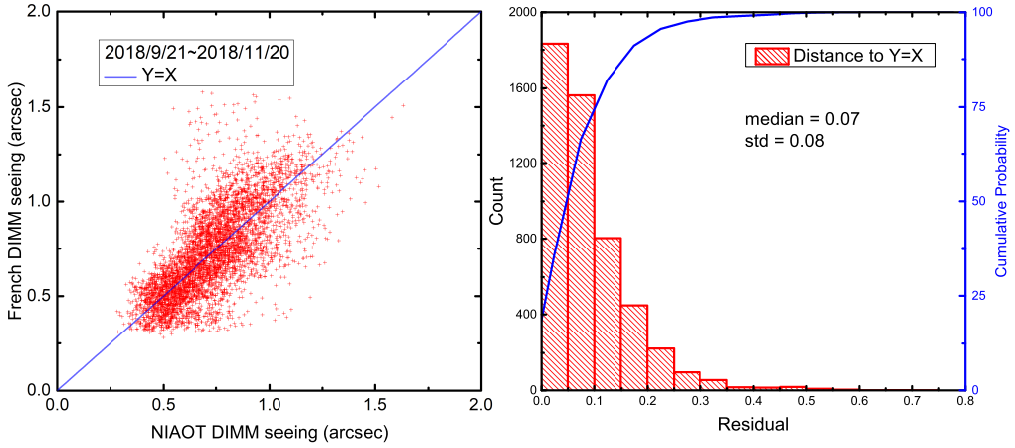

Fig. 4 Comparison result of two DIMMs at 11 m. *Left panel*: correlation between NIAOT DIMM and French DIMM. *Right panel*: distribution and cumulative distribution function of residuals.

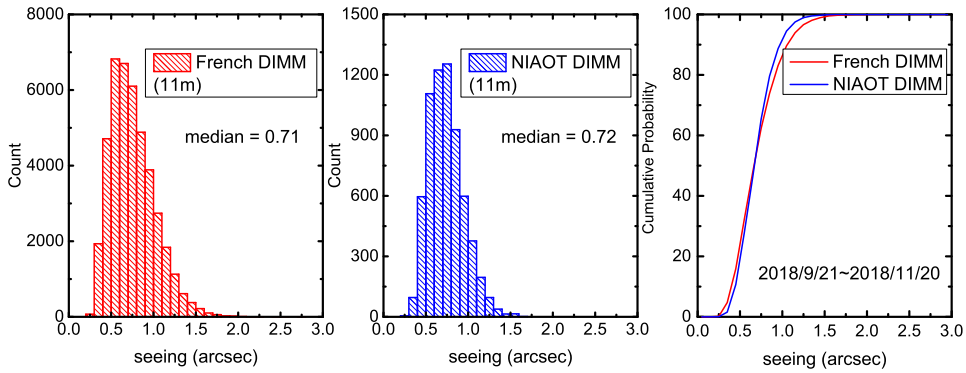

Fig. 5 Seeing distributions and cumulative distribution functions from two DIMMs over the period from 2018 September 21 to 2018 November 20 at 11 m.

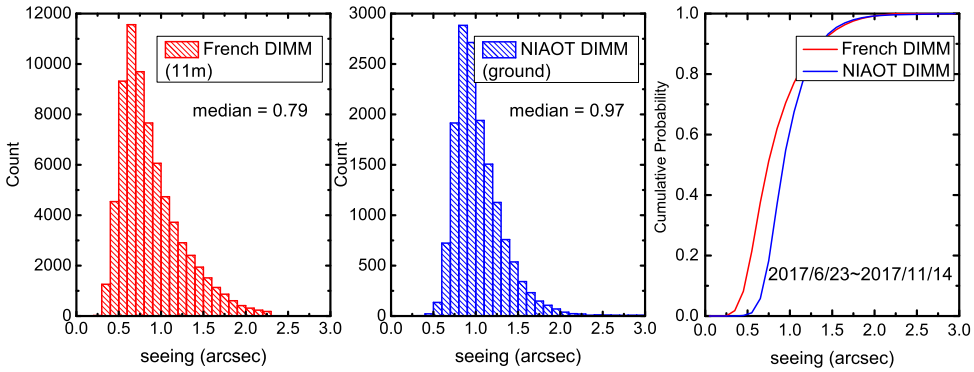

Fig. 6 Seeing distributions and cumulative distribution functions from two DIMMs during the period from 2017 June 23 to 2017 November 14 at 11 m and on the ground level.

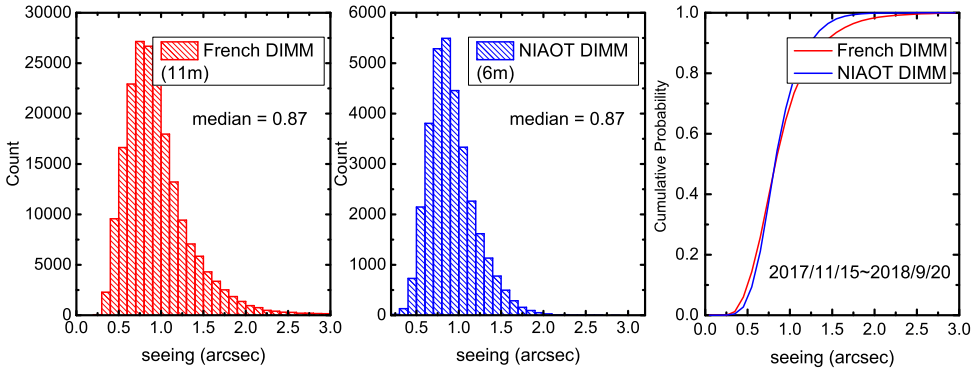

Fig. 7 Seeing distributions and cumulative distribution functions from two DIMMs during the period from 2017 November 15 to 2018 September 20 at 11 m and 6 m.

five values as the value of the French DIMM. The comparison result of two DIMMs during this period is plotted in Figure 4, in which the correlation of the NIAOT DIMM and the French DIMM and the statistical analysis of the residuals for the line $Y = X$ are displayed. The median of the residuals is 0.07 and the standard variance is 0.08, which indicates that the difference between the two DIMMs is very small. The seeing distributions and cumulative distribution functions during this period are shown in Figure 5. The median seeing values of the French DIMM and NIAOT DIMM are 0.71 arcsec and 0.72 arcsec respectively.

4.2 Seeing at Different Heights

During the whole measurement period, we operated two DIMMs at different heights to explore the distribution of near-ground turbulence. In order to eliminate the influence of the occasional failure of the two DIMMs on results, we only include the data from nights during which both DIMMs were working normally. From 2017 June 23 to 2017 November 14, the NIAOT DIMM was put on the ground while the French DIMM was on the 11-meter tower. In Figure 6, we present the distributions and cumulative distribution function curves of the seeing values acquired during this period. The median value from the French DIMM is 0.79 arcsec at 11 m and the median value from the NIAOT DIMM is 0.97 arcsec at the ground level.

In autumn 2017, we built a 6-meter tower, and the NIAOT DIMM was moved to the top of this 6-meter tower on 2017 November 15. The seeing acquired from the NIAOT DIMM at 6 m lasted until 2018 September 20. The results of measurement during this period are displayed in Figure 7. Both of the median seeing values at the two heights are 0.87 arcsec. The difference between seeing median at 11 m and ground level is 0.18 arcsec, and the difference is very small, between 11 m and 6 m, indicating that the near-ground turbulence is concentrated in the area below 6 m from the ground at the Muztagh-ata site.

4.3 Seeing at 11 Meters

From 2017 June 23 to 2018 November 20, there were 293 nights in total available for seeing data and 142 nights dur-

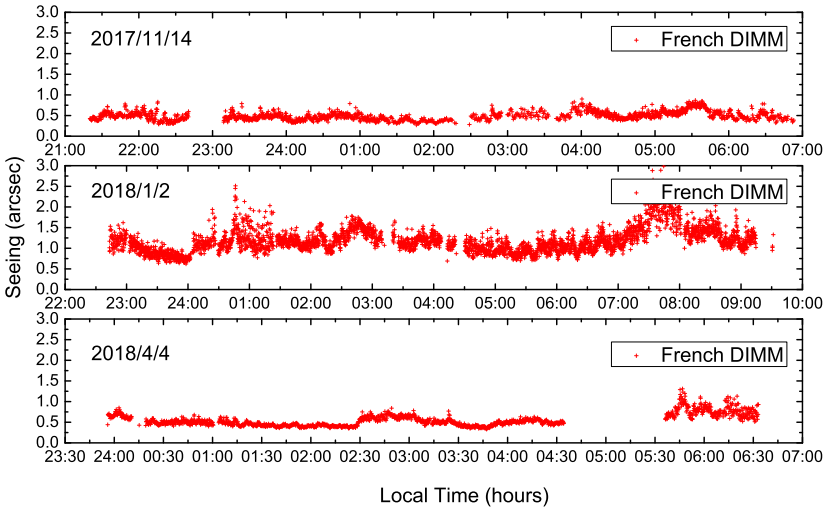

Fig. 8 Example of French DIMM seeing values during observable nights. Good steady night (2017–11–14), erratic night (2018–01–02) and degraded night (2018–04–04) from top to bottom respectively.

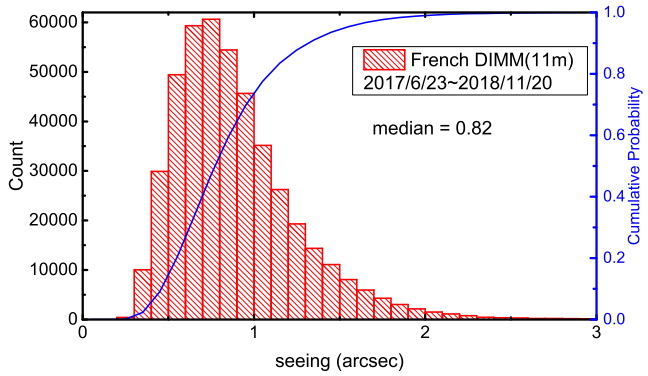

Fig. 9 Seeing distributions and cumulative functions from French DIMM at 11 m during period of 2017 June 23 to 2018 November 18.

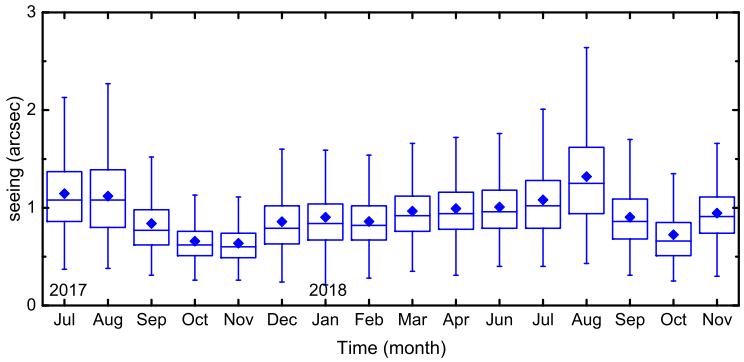

Fig. 10 Monthly statistics on seeing from July 2017 to November 2018 (there were no data in May 2018 because the tower was being rebuilt). Each *box* represents the values in the range of 25% to 75% and the associated *vertical line* signifies the values ranging from 1% to 99%. The *diamonds* and *horizontal lines* inside every *box* correspond to mean and median values respectively.

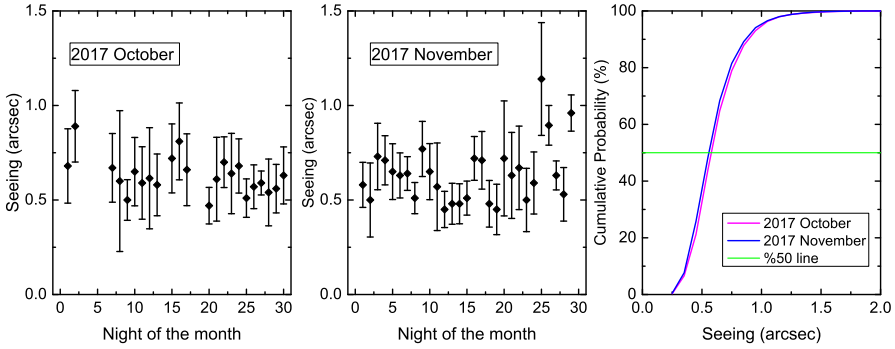

Fig. 11 *Left and middle panels*: Median seeing values (with lower and upper limits represented by first and third quartiles respectively) for each night of October 2017 and November 2017. *Right panel*: Seeing Cumulative Distribution Function and 50% line for the two months (pink for October 2017 and blue for November 2017).

ing which more than 75% of the time the instruments acquired data. Figure 8 shows three seeing cases of the 142 nights: good steady nights, with excellent seeing throughout the night (standard variance value less than 0.25 and median value less than 0.82, 66 good steady nights in total, 2017 November 14 for example); erratic seeing night, with irregular seeing throughout the night (standard variance greater than 0.25, 40 erratic nights in total, 2018 January 2 for example); degraded night in which there is a sudden burst of bad seeing (the standard variance value becomes greater than 0.25 toward dawn, 2018 April 4 for example).

The French DIMM median seeing value at 11 m from 2017 June 23 to 2018 November 20 was 0.82 arcsec as plotted in Figure 9. We have conducted a monthly analysis of all available data. There were 16 months from July 2017 to November 2018 available for seeing measurements, but no seeing values during May 2018 because the 11-meter tower was being rebuilt. The boxplot in Figure 10 depicts the seeing monthly behavior in the period, in which each box represents the values in the range of 25% to 75% and the associated vertical line signifies the values ranging from 1% to 99%, and the diamonds and horizontal lines inside every box correspond to mean and median values respectively. From Figure 10, we can ascertain that the best time period for seeing at the Muztagh-ata site is from late autumn to early winter. The nightly seeing statistics and cumulative distribution functions during October and November 2017 are displayed in Figure 11. The median values are 0.62 arcsec and 0.60 arcsec respectively for these two months. Bad seeing nights appeared frequently in July and August every year, mainly due to the erratic weather during autumn.

In order to explore the seeing behavior throughout the night, we plot the hourly results for each season integrated over this acquisition period in Figure 12 (spring, summer, autumn and winter from top to bottom respectively). The solid lines and pluses indicate the median seeing values in each hour (UT time), the dashed lines signify 25% and 75%, and the asterisks represent the amount of data. In spring, summer and winter, the seeing becomes worse toward dawn, but in autumn it manifests a change that deteriorates first and then improves. It is obvious that the seeing during the second half of the night in autumn is better than during the first half.

5 SEEING DEPENDENCE ON METEOROLOGICAL CONDITIONS

One automated weather station named second generation Kunlun Automated Weather Station (KLAWS-2G)[1] was installed at the Muztagh-ata site and started to record data from 2017 August 1. It has several high precision temperature sensors (Young 4-wire RTD, Model 41342), cup anemometers and wind vanes at different heights, which make it possible to explore the influence of meteorological parameters on seeing. In this section, the seeing data we consider are from the French DIMM in the period of 2017 August 1 to 2018 November 20 at 11 m.

5.1 Temperature Inversion

The phenomenon of temperature inversion means air temperature decreases with decreasing elevation. It comes with stable atmospheric structure. Hu et al. (2014, 2019) used KLAWS-2G and found strong temperature inversion occurs frequently at Dome A (Burton 2010). We want to explore the lasting time and influence on seeing at Muztagh-ata. Figure 13 depicts the statistics of an inversion layer in two periods: one is in the afternoon from 13:00 to 15:00 (UTC+8), another is past midnight from 1:00 to 3:00 (UTC+8), which we will call “midnight”. It can be seen that in 70% of the time during the midnight period, the

[1] `http://aag.bao.ac.cn/xjtest/index.php`

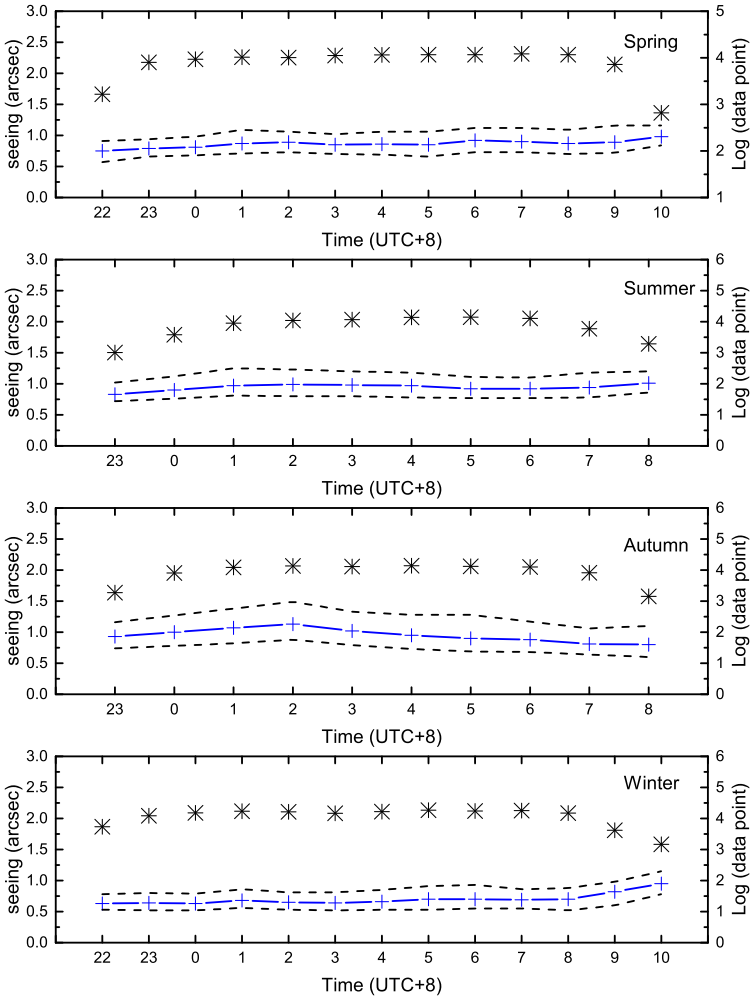

Fig. 12 Hourly seeing statistics for each season (spring, summer, autumn and winter from top to bottom respectively). The *solid lines* and *pluses* indicate the median seeing values at each hour (UT time), and the *dashed lines* indicate 25% and 75%. *Asterisks* mark the amount of data in each hour.

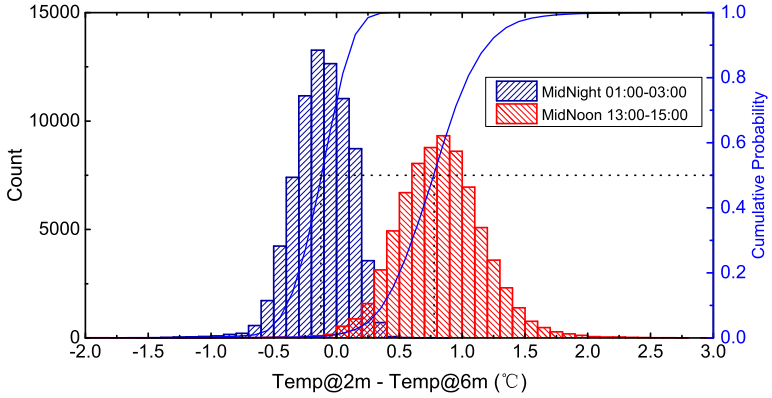

Fig. 13 The distribution and cumulative distribution functions of the difference between the temperature at 2 m and 6 m in two periods: 13:00 15:00 (UTC+8) afternoon (*red*) and 1:00∼3:00 (UTC+8) at night (*blue*).

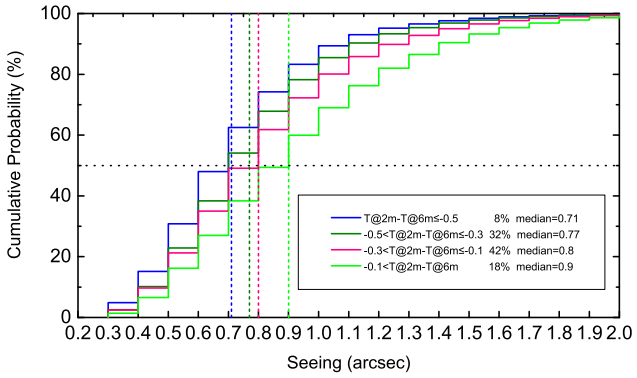

Fig. 14 Cumulative distribution functions of seeing in four ranges of the difference between the temperatures at 2 m and 6 m: smaller than -0.5°C (*blue*), $-0.5 \sim -0.3^{\circ}$C (*dark green*), $-0.3 \sim -0.1^{\circ}$C (*pink*) and higher than -0.1°C (*light green*).

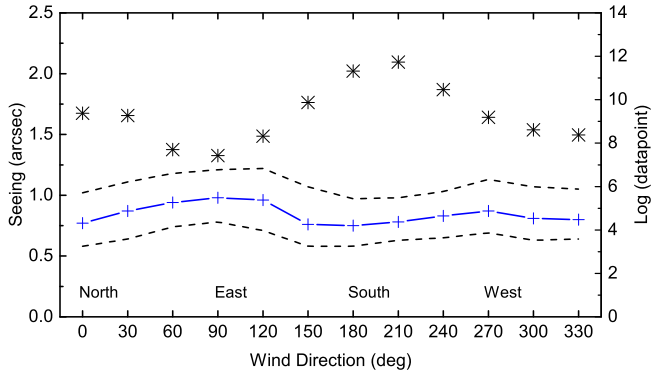

Fig. 15 The *solid line* and *crosses* indicate the median seeing values in each 30° wind direction bin, and the *dashed lines* signify 25% and 75%. *Asterisks* mark the amount of data in each bin.

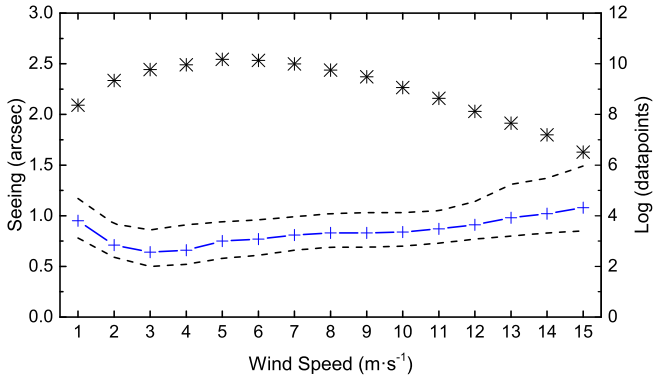

Fig. 16 Seeing statistics at various wind speeds (wind direction from 180° to 270°). Wind speeds were binned in 1 $\mathrm{m\,s^{-1}}$ intervals. The *solid line* and *pluses* indicate the median seeing values at various wind speeds, and the *dashed lines* signify 25% and 75%. *Asterisks* mark the amount of data in each bin.

temperatures at 2 m are smaller than those at 6 m, and the median value of the difference is -0.2°C.

The relationship between seeing and temperature inversion is presented in Figure 14. There are four cumulative distribution function curves in the plot representing four ranges of the difference between the temperatures at 2 m and 6 m. The blue one is the range smaller than -0.5°C with median seeing value 0.71 arcsec. Dark green is the range -0.5 to -0.3°C with median seeing value 0.77 arcsec. Pink is the range -0.3 to -0.1°C with

seeing median value 0.8 arcsec. Light green is the range higher than -0.1°C with median seeing value 0.9 arcsec. Figure 14 demonstrates that stronger inversion can bring better seeing.

5.2 Wind

We use the sensors homed at an altitude of 10 m for analysis of the seeing versus wind speed and direction. Figure 15 and Figure 16 show the relation of the seeing measurements to wind direction and speed of prevailing wind direction. According to the meteorological parameter measurement results at the Muztagh-ata site for this site-testing task, the prevailing wind is southwest in this area (Xu et al. 2020a,b). The asterisks in Figure 15 represent the amount of seeing data in every 30° of wind direction. The largest amount of data occurs in 180° to 240° (prevailing wind direction). There is a clear bottom in the amount of data and a clear peak in median seeing value with east winds. This indicates that the east winds bring about local weather changes and unstable ground turbulence.

Figure 16 plots the relation of seeing and southwest wind speed (wind direction from 180° to 270°). The asterisks mark the amount of data and solid line and pluses indicate the median seeing values. With the increase of wind speed, the median seeing value manifests an initial drop until the wind speed reaches $3\,\mathrm{m\,s^{-1}}$ then keeps growing. When the wind speed is greater than $12\,\mathrm{m\,s^{-1}}$, the amount of data decreases sharply and the 75% line deviates from the median line. From these two figures, we can see that the most stable ground turbulence occurs with southwesterly wind speed at $3\,\mathrm{m\,s^{-1}}$.

6 CONCLUSIONS

DIMM data collected from June 2017 to November 2018 at the Muztagh-ata site have been presented. We want to acquire some preliminary conclusion regarding near-ground turbulence distribution and seeing condition at our site. The main results yielded from this work are as follows:

1. The seeing median value at 11 m during the whole measurement period is 0.82 arcsec. The difference in seeing between the 11-meter level and 6-meter level is very small but significant between the 6-meter level and ground level. This illustrates that the near-ground turbulence is concentrated within 6 m above the ground at the Muztagh-ata site.

2. Seasonal statistics demonstrate that the best season for optical astronomical observation at the Muztagh-ata site is from late autumn to early winter. Autumn is relatively bad for seeing because of erratic weather. Hourly analysis shows that there is a tendency for seeing that becomes progressively worse toward dawn in most times of the year, but in autumn, the seeing deteriorates first and then improves during night.

3. The dependence of the seeing at 11 m on meteorological conditions is discussed. We calculate the frequency of temperature inversion during midnight, and 70% of that time the inversion was present. Then we analyze the relationship between inversion and seeing. Results present evidence that stronger inversion can bring better seeing.

4. We present seeing statistics at various wind speeds of prevailing wind direction, from which the conclusion would be made that stable ground turbulence occurs when there is a stable breeze from the southwest.

Acknowledgements This work is supported by the National Nature Science Foundation of China (Grant Nos. 11873081 and 11603065), and the Operation, Maintenance and Upgrading Fund for Astronomical Telescopes and Facility Instruments, budgeted from the Ministry of Finance of China (MOF) and administered by the Chinese Academy of Sciences.

References

Burton, M. G. 2010, A&A Rev., 18, 417
Cao, Z. H., Liu, L. Y., Zhao, Y. H., et al. 2020a, RAA (Research in Astronomy and Astrophysics), 20, 81
Cao, Z. H., Hao, J. X., Feng, L., et al. 2020b, RAA (Research in Astronomy and Astrophysics), 20, 82
Els, S. G., Schöck, M., Bustos, E., et al. 2009, PASP, 121, 922
Feng, L., Hao, J. X., Cao, Z. H., et al. 2020, RAA (Research in Astronomy and Astrophysics), 20, 80
Hu, Y., Shang, Z., Ashley, M. C. B., et al. 2014, PASP, 126, 868
Hu, Y., Hu, K., Shang, Z., et al. 2019, PASP, 131, 015001
Michel, R., Echevarría, J., Costero, R., & Harris, O. 2003, Revista Mexicana de Astronomia y Astrofisica Conference Series, 19, 37
Roddier, F. 1981, Progess in Optics, 19, 281
Sarazin, M., & Roddier, F. 1990, A&A, 227, 294
Skidmore, W., Els, S., Travouillon, T., et al. 2009, PASP, 121, 1151
Sánchez, L. J., Cruz-González, I., Echevarría, J., et al. 2012, MNRAS, 426, 635
Tian, J. F., Deng, L. C., Zhang, X. B., et al. 2016, PASP, 128, 105003
Tokovinin, A. 2002, PASP, 114, 1156
Wang, J. F., Tian, J. F., Zeng, X. Q., et al. 2020, RAA (Research in Astronomy and Astrophysics), 20, 83
Xu, J., Esamdin, A., Hao, J. X., et al. 2020a, RAA (Research in Astronomy and Astrophysics), 20, 86
Xu, J., Esamdin, A., Feng, G. J., et al. 2020b, RAA (Research in Astronomy and Astrophysics), 20, 88